ELSEVIER

www.elsevier.nl/locate/jorganchem

Journal of Organometallic Chemistry 588 (1999) 176–185

Journal of Organometallic Chemistry

Force-field parameterisation, synthesis and crystal structure of a novel tricarbonylchromium arene complex

Samantha J. Hughes [a], John R. Moss [a,1], Kevin J. Naidoo [a,*], Janet F. Kelly [b], Andrei S. Batsanov [b]

[a] *Department of Chemistry, University of Cape Town, Rondebosch 7701, South Africa*
[b] *Department of Chemistry, University of Durham, Durham, UK*

Received 1 January 1999; received in revised form 1 June 1999

Abstract

We construct a force field for organochromium poly(benzyl phenyl ether) dendrimers from reported experimental data and experimental data measured by us. Potential function terms are principally optimised through the use of crystal structure data of a novel $[Cr(CO)_3(C_6H_5CH_2OCH_2C_6H_5)Cr(CO)_3]$ complex. We report the synthesis and the crystal structure data of the chromium complex. In addition the important benzyl ether linkage torsion angle parameter is optimized by comparison with ab initio torsional data of a model compound. With this information, a force field suitable for molecular mechanics and dynamics calculations of organochromium poly(benzyl phenyl ether) dendrimers is constructed. The force field is tested by mapping the energy surface and simulating the crystal structure of $[Cr(CO)_3(C_6H_5CH_2OCH_2C_6H_5)Cr(CO)_3]$.

Keywords: Dendrimers; Tricarbonylchromium arene complexes; Parameterisation; Force field; Molecular mechanics; Ab initio; Crystal structure

1. Introduction

Incorporation of metals into a dendritic architecture has resulted in the preparation of dendrimers with a wide range of properties, enabling their use as liquid crystals [1], catalysts [2,3] and inorganic sensors [3]. Recently, an increasing amount of interest has been focused on the synthesis of novel organometallic dendrimers [1–8]. Previous work done in our laboratories has led to the synthesis of new iron and ruthenium dendrimers, based on the poly(benzyl phenyl ether) class of dendrimer [9]. We have also examined the functionalisation of the peripheral aromatic rings as (arene)tricarbonylchromium(0) complexes (Fig. 1) as has been done for polysilane dendrimers [10].

The fractal nature of these macromolecules leads to difficulties in obtaining suitable crystals, thus precluding the use of X-ray methods for all but the lowest-generation dendrimers. Computational techniques have been used to study these complex macromolecules [11–16]. While most of these calculations involved coarse-grained methods, only a limited number of comprehensive investigations using force-field methods on dendrimers have been reported [17,18]. Furthermore, no computational studies of any organometallic dendrimers have been reported. However, we have recently completed an exhaustive study on the structure of organic dendrimers and the corresponding organochromium poly(benzyl phenyl ether) dendrimers, by molecular mechanics and dynamics techniques [19], using the program CHARMM [20]. These calculations were only possible through the development of a force field for these dendrimers, which we report here. The development of the force field rests largely on the extension of an existing CHARMM force field [21,22] to include parameters for the treatment of the organometallic moieties.

Two necessary parts of the force field were absent from existing data and required development. First all parameters related to the (arene)tricarbonyl-

* Corresponding author. Fax: +27-21-6897499.
E-mail address: knaidoo@psipsy.uct.ac.za (K.J. Naidoo)
[1] Also corresponding author.

0022-328X/99/$ - see front matter
PII: S0022-328X(99)00372-1

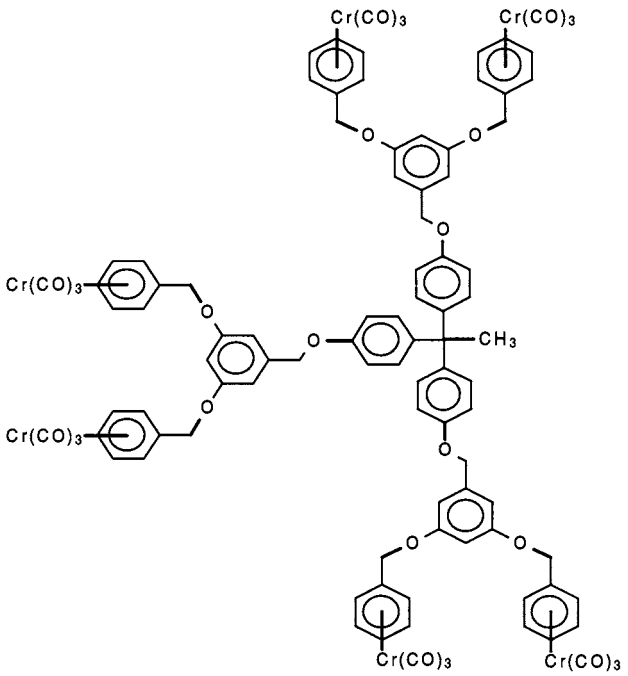

Fig. 1. A first-generation organochromium dendrimer.

chromium(0) complex were needed. For this purpose we synthesised, crystallised and solved the crystal structure of a model compound $[Cr(CO)_3(C_6H_5CH_2OCH_2C_6H_5)Cr(CO)_3]$ (**2**). We then used the data to build a parameter set. Secondly the CHARMM polymer force field [22] under development in our laboratory lacked rotational ether linkage dihedral angle parameters. The ether linkage is central to the structure and conformation of the poly(benzyl phenyl ether) class of dendrimers. We used data generated from ab initio calculations to develop these CHARMM parameters.

We report the synthesis of $[Cr(CO)_3(C_6H_5CH_2OCH_2C_6H_5)Cr(CO)_3]$ (**2**) in Section 2 and the crystal structure of this compound in Section 3. We then discuss the parameterization procedure in Section 4. We compare the results of a conformational energy surface, which we constructed, to experimental crystal structure conformations in Section 5.1. In Section 5.2 we report two test calculations where we have simulated crystal structures of the chromium complex using (a) the experimental and (b) the computer-predicted low-energy conformations.

2. Synthesis of $(C_6H_5CH_2OCH_2C_6H_5)[Cr(CO)_3]_2$

The peripheral groups of the organochromium dendrimers are (benzyl ether) tricarbonylchromium complexes. The structures of simple benzylic ether tricarbonylchromium complexes could be used in the parameterisation of the force field, however the Cambridge Structural Database [23] contained no such examples. It was therefore necessary, as part of the parameterisation effort, to synthesise and solve the structure of a model (arene)tricarbonylchromium complex. We prepared the novel compound $[Cr(CO)_3(C_6H_5CH_2OCH_2C_6H_5)Cr(CO)_3]$ (**2**) by direct complexation of dibenzyl ether with chromium hexacarbonyl (Scheme 1). The desired product was obtained in 49% yield, along with the intermediate monometallic species $[Cr(CO)_3(C_6H_5CH_2OCH_2C_6H_5)]$ (**3**) in 34% yield. This intermediate **3** is a known compound, previously synthesised via a different route [24].

2.1. General synthesis data

All manipulations were carried out under a nitrogen atmosphere by using standard Schlenk techniques. Re-

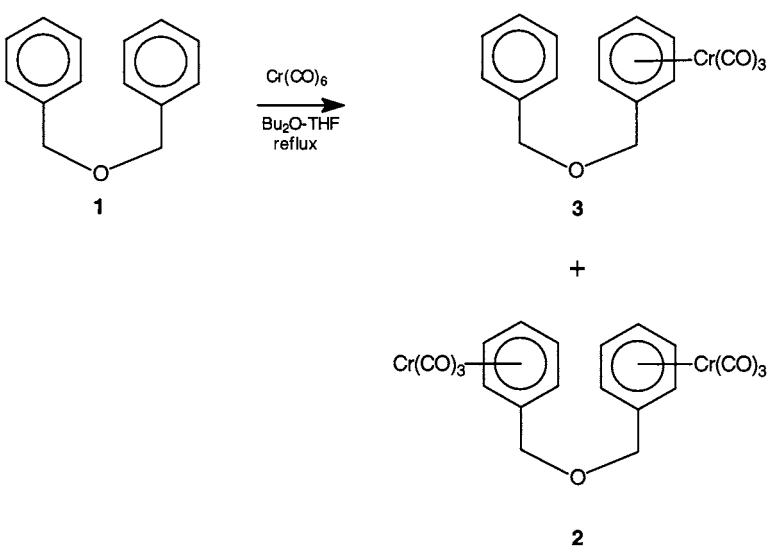

Scheme 1.

actions involving chromium carbonyl derivatives were protected from light. Dibenzyl ether and THF were dried over sodium–benzophenone and distilled prior to use. Chromium hexacarbonyl was purchased from Strem Chemicals and used without further purification. Column chromatography was conducted with Merck Kieselgel (230–400) mesh.

IR spectra were recorded in solution on a Perkin–Elmer Paragon 1000 FT-IR spectrometer. ^{1}H-NMR spectra were recorded on a Varian Unity Spectrometer (400 MHz). ^{13}C-NMR spectra were recorded on the same instrument at 100 MHz. Tetramethylsilane was used as a reference standard in both cases. Melting points were measured using a Reichert Thermovar hot-stage microscope and are uncorrected. Microanalyses were determined at the University of Cape Town, using a Fisons EA 1108 CHNS-O instrument. Mass spectra were recorded on a VG micromass 16F spectrometer operating at 70 eV with an accelerating voltage of 4 kV and a variable source temperature.

2.2. Preparation of $[Cr(CO)_3(C_6H_5CH_2OCH_2C_6H_5)Cr(CO)_3]$ (2)

Chromium hexacarbonyl (2.43 g, 11.0 mmol) was added to a stirred solution of dibenzyl ether **1** (1 cm^3, 5.26 mmol) in a mixture of dibutyl ether (45 cm^3) and THF (4 cm^3) and the resulting yellow solution was refluxed for 29 h. A further portion of chromium hexacarbonyl (0.50 g, 2.3 mmol) was then added, and the mixture was refluxed for 3 h in an attempt to force the reaction to completion, but the reaction was stopped when signs of decomposition were observed. The solution was allowed to cool and the solvent was removed under reduced pressure. The resulting residue was dissolved in CH_2Cl_2 and filtered through Celite® to give a clear yellow solution. The solvent was evaporated under reduced pressure to give a yellow solid along with some decomposition products (2.251 g). This mixture was flash chromatographed on silica gel (80 g) eluting with toluene–hexane (9:1) to give (dibenzyl ether)tricarbonylchromium(0) [24] (**3**) as a yellow oil (216 mg), followed by mixed fractions. The mixed fractions were flash chromatographed on silica gel (150 g), eluting with toluene–hexane (9:1) to afford a further portion of **3** (374 mg, 34% combined). IR (hexane) ν(CO) 1981 (vs) and 1913 (vs) cm^{-1}. MS: m/z 334 [M$^+$]. ^{1}H-NMR ($CDCl_3$) δ(ppm): 4.17 (2H, s, ArCH_2O), 4.55 (2H, s, ArCH_2O), 5.15–5.30 (5H, m, ArH), 7.15–7.30 (5H, m, ArH). ^{13}C-NMR ($CDCl_3$) δ(ppm): 70.2 (ArCH$_2$O), 73.0 (ArCH$_2$O), 91.5 (*p*-*C*), 92.0, 92.8 (*o*- and *m*-*C*), 107.9 (*ipso*-*C*), 127.9 (*p*-*C*), 127.7, 128.5 (*o*- and *m*-*C*), 137.4 (*ipso*-*C*), 232.6 (*C*O).

Further elution afforded the product **2** (1.199 g, 48.5%). M.p. 126–127°C (CH_2Cl_2/hexane). Anal. Found: C, 51.1; H, 2.95%. M$^+$ 470. $C_{20}H_{14}Cr_2O_7$. Calc. C, 51.1; H, 3.0%. M 470. IR (CH_2Cl_2) ν(CO) 1970 (vs) and 1890 (vs) cm^{-1}. ^{1}H-NMR ($CDCl_3$) δ(ppm): 4.36 (4H, s, ArCH_2O), 5.26–5.44 (10H, m, ArH). ^{13}C-NMR δ(ppm): 70.4 (*C*H$_2$O), 93.7 (*p*-*C*), 93.8, 94.8 (*o*- and *m*-*C*), 111.0 (*ipso*-*C*), 191.1 (*C*O).

3. Crystal structure

A crystal of $[Cr(CO)_3(C_6H_5CH_2OCH_2C_6H_5)Cr(CO)_3]$ suitable for single-crystal diffraction data collection, was grown by slow evaporation from CH_2Cl_2–hexane. The crystal appeared to be a pseudo-merohedral twin with the twinning law $-h, -k, l$; the contribution of the second component was refined to 0.073(1). All the measurements were performed at 150 K on a 3-circle Bruker axs SMART diffractometer, with a CCD area detector, using graphite monochromated Mo–K$_\alpha$ radiation. A total of 17 533 reflections (4315 unique) with $\theta < 27.5$ were measured, of which 3340 were observed [$I > 2\sigma(I)$]. The crystal was shaped as a platelet with approximate dimensions $0.4 \times 0.3 \times 0.02$ mm^3 and required an empirical absorption correction carried out with the SADABS program [25]. The minimum and maximum corrections were 0.73 and 1.00, respectively. Crystal decay was monitored by repeating the initial 50 frames at the end of the data collection and analyzing the 205 duplicate reflections.

The structure was solved by direct methods, followed by Fourier difference syntheses. Full matrix least-squares refinement was carried out against F^2 of all data using the SHELXTL software [26]. PLUTO was used for the molecular plotting [27]. The hydrogen atoms were located using the geometrical method of AFIX instruction in the SHELXL-93 program [26] and then allowed to refine freely.

The weighting scheme employed was of the form $w = 1/[\delta^2 F_o^2 + (0.0393P)^2 + 7.6327P]$ where $P = (F_o^2 + 2F_c^2)/3$. The crystallographic data together with data collection details are given in Table 1.

3.1. Structural analysis of $[Cr(CO)_3(C_6H_5CH_2OCH_2C_6H_5)Cr(CO)_3]$ (2)

The structure of $[Cr(CO)_3(C_6H_5CH_2OCH_2C_6H_5)Cr(CO)_3]$ (**2**) was established by single-crystal X-ray diffraction analysis. The molecular structure is shown in Fig. 2 and selected bond lengths and angles are given in Table 2. The complex displays the classic piano-stool structure [28]. The aromatic rings are planar, with the Cr atoms situated directly beneath the ring centroids, at distances of 1.72 and 1.71 Å. In monosubstituted chromium arene complexes, the tricarbonyl tripod usually adopts one of two conformations in relation to the ring: *anti* eclipsed or *syn* eclipsed, depending

Table 1
Crystal data and structure refinement for **2**

Empirical formula	$C_{20}H_{14}Cr_2O_7$
Formula weight	470.31
Temperature (K)	150(2)
Wavelength (Å)	0.71073
Crystal system	Monoclinic
Space group	$P12_1/n1$
Unit cell dimensions	
a (Å)	7.6250(5)
b (Å)	10.5321
c (Å)	23.562(2)
α (°)	90
β (°)	90.613(4)
γ (°)	90
V (Å^3)	1892.1(2)
Z	4
D_{calc} (g cm^{-3})	1.651
Absorption coefficient (mm^{-1})	1.189
$F(000)$	952
Crystal size (mm^3)	$0.4\times0.3\times0.02$
θ range for data collection	$0.86°<\theta<27.49°$
Index ranges	$-9\le h\le 9,\ -13\le k\le 13,$ $-30\le l\le 27$
Reflections collected	17533
Independent reflections	4315 [$R_{int}=0.0674$]
Observed reflections [$I>2\sigma(I)$]	3340
Absorption correction	Multi-scan (SADABS)
Max. and min. transmission	1.00 and 0.73
Refinement method	Full-matrix least-squares on F^2
Data/restraints/parameters	4311/0/319
Goodness-of-fit on F^2	1.072
Final R indices [$I>2\sigma(I)$]	$R_1=0.0528$ $wR_2=0.1190$
R indices (all data)	$R_1=0.0795$ $wR_2=0.1386$
Largest shift/estimated S.D. ratio	−0.001
Largest difference peak and hole (e Å^{-3})	0.593, −0.611

on whether the substituent is electron withdrawing or donating, respectively [28]. In this present structure, only one of the rings (C11–C16) adopts the expected *anti* eclipsed conformation, the other ring (C21–C26) being staggered. There is precedent for monosubstituted arene complexes adopting the staggered conformation due to strong steric effects [28], but it is not clear whether steric reasons are the cause in this instance. Fig. 2(a) and (b) illustrates the conformation of the two aromatic rings in the dibenzyl ether bis-complex (view down centroid–Cr axis). The staggered ring displays significant bond length variation, with the carbon–carbon bonds situated above the carbonyl ligands, lengthened by an average value of 0.023 Å. The *anti* eclipsed complexed ring shows no significant bond length variation.

4. Force-field parameterisation

Molecular mechanics is based on a classical mechanics force-field description of a molecule. In general the atoms making up a molecule are defined as spheres of varying sizes and charges in an attempt to adequately describe their electronic states. The van der Waals and Coulombic terms (non-bonded terms) describe these atomic physical properties. The parameters for the non-bonded terms are taken from existing CHARMM force fields [21].

A standard harmonic potential function is employed to describe the bond stretching motion:

$$E_b = \Sigma\, k_b(r - r_0)^2 \quad (1)$$

where r_0 is the equilibrium value of the bond length (Å) and k_b is in kcal mol^{-1} Å^{-2}. The bond angle bending is also described using a harmonic approximation:

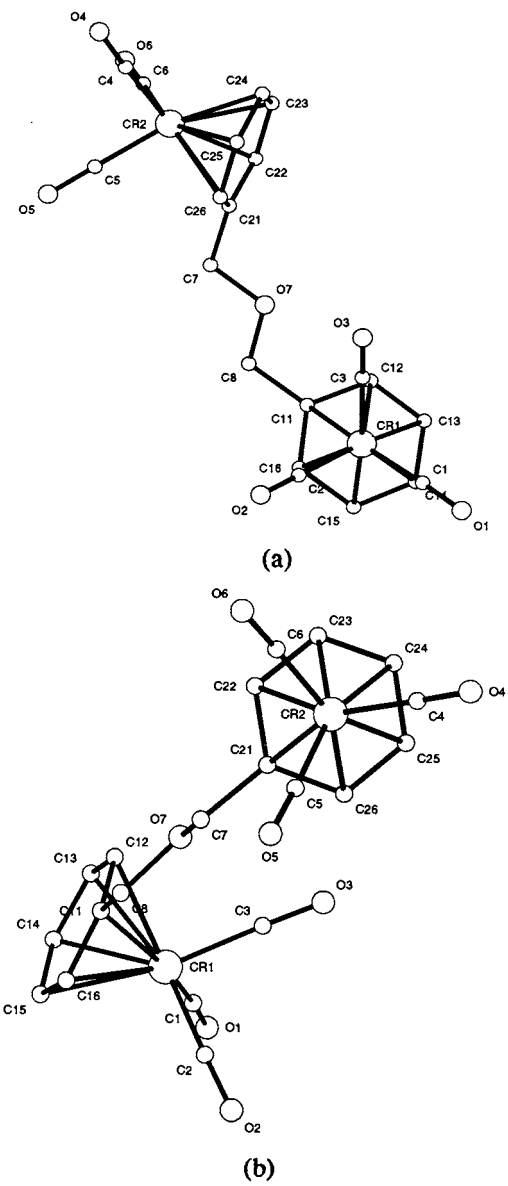

Fig. 2. (a) The crystal structure of $[Cr(CO)_3(C_6H_5CH_2OCH_2C_6H_5)Cr(CO)_3]$ (**2**), (view down Cr1-centroid axis). (b) $[Cr(CO)_3(C_6H_5CH_2OCH_2C_6H_5)Cr(CO)_3]$ (**2**), (view down Cr2-centroid axis).

Table 2
Selected bond lengths (Å) and angles (°) for **2**

Bond lengths (Å)			
Cr(1)–C(1)	1.843(5)	Cr(1)–C(3)	1.850(5)
Cr(1)–C(2)	1.854(5)	Cr(1)–C(16)	2.202(4)
Cr(1)–C(12)	2.222(5)	Cr(1)–C(13)	2.225(5)
Cr(1)–C(15)	2.227(5)	Cr(1)–C(14)	2.228(5)
Cr(1)–C(11)	2.239(4)	Cr(2)–C(5)	1.845(5)
Cr(2)–C(6)	1.856(5)	Cr(2)–C(4)	1.856(5)
Cr(2)–C(22)	2.205(5)	Cr(2)–C(21)	2.209(5)
Cr(2)–C(23)	2.213(5)	Cr(2)–C(24)	2.236(5)
Cr(2)–C(26)	2.239(5)	Cr(2)–C(25)	2.240(5)
O(1)–C(1)	1.161(6)	O(2)–C(2)	1.155(6)
O(3)–C(3)	1.153(6)	O(4)–C(4)	1.151(6)
O(5)–C(5)	1.155(6)	O(6)–C(6)	1.154(6)
Centroid–Cr(1)	1.72 [a]	Centroid–Cr(2)	1.71 [a]
O(7)–C(7)	1.413(6)	O(7)–C(8)	1.429(6)
C(8)–C(21)	1.499(7)	C(7)–C(11)	1.515(6)
C(11)–C(12)	1.412(7)	C(11)–C(16)	1.419(7)
C(12)–C(13)	1.413(7)	C(13)–C(14)	1.389(8)
C(14)–C(15)	1.402(7)	C(15)–C(16)	1.416(6)
C(21)–C(22)	1.417(7)	C(21)–C(26)	1.427(6)
C(22)–C(23)	1.412(8)	C(23)–C(24)	1.401(8)
C(24)–C(25)	1.427(8)	C(25)–C(26)	1.379(7)
Bond angles (°)			
C(1)–Cr(1)–C(3)	91.0(2)	C(1)–Cr(1)–C(2)	88.5(2)
C(3)–Cr(1)–C(2)	86.1(2)	C(5)–Cr(2)–C(6)	84.5(2)
C(5)–Cr(2)–C(4)	90.0(2)	C(6)–Cr(2)–C(4)	89.2(2)
C(7)–O(7)–C(8)	111.3(4)	O(1)–C(1)–Cr(1)	177.0(4)
O(2)–C(2)–Cr(1)	178.1(4)	O(3)–C(3)–Cr(1)	178.5(4)
O(4)–C(4)–Cr(2)	178.6(5)	O(5)–C(5)–Cr(2)	176.7(5)
O(6)–C(6)–Cr(2)	177.0(4)	O(7)–C(8)–C(21)	107.7(4)
O(7)–C(7)–C(11)	109.6(4)	C(12)–C(11)–C(16)	119.0(4)
C(12)–C(11)–C(7)	121.3(4)	C(16)–C(11)–C(7)	119.6(4)
C(11)–C(12)–C(13)	120.5(5)	C(14)–C(13)–C(12)	120.1(5)
C(13)–C(14)–C(15)	120.5(5)	C(14)–C(15)–C(16)	120.1(5)
C(15)–C(16)–C(11)	119.8(4)	C(22)–C(21)–C(26)	119.1(4)
C(22)–C(21)–C(8)	120.2(4)	C(26)–C(21)–C(8)	120.6(5)
C(23)–C(22)–C(21)	119.8(5)	C(24)–C(23)–C(22)	120.9(5)
C(23)–C(24)–C(25)	118.9(5)	C(26)–C(25)–C(24)	120.9(5)
C(25)–C(26)–C(21)	120.4(5)	C_{ring}–Centroid–Cr(2)	90.2, 89.8 [a,b]
C_{ring}–Centroid–Cr(2)	90.0, 90.0 [a,b]		

[a] Errors are not available for these measurements.
[b] Two values are indicated because there are two average values for that parameter due to bond length alternation in the aromatic ring.

$$E_\theta = \Sigma\, k_\theta(\theta - \theta_0)^2 \quad (2)$$

where θ_0 is the value of the angle at equilibrium and k_θ is in kcal mol^{-1} rad^{-2}.

A Fourier term (Eq. (3)) approximates the energy associated with torsional rotation (n is the periodicity and can take on values of 1–6):

$$E_\phi = \Sigma\, |k_\phi| - k_\phi \cos(n\phi) \quad (3)$$

The force constant k_ϕ is in kcal mol^{-1} rad^{-2} and the dihedral angle ϕ is in degrees.

No improper torsion angles were included in the description of the organometallic species. We used parameters from existing CHARMM force fields [22,21] for bonds, angles and dihedrals not directly related to the chromium ion.

4.1. Development of (arene)tricarbonylchromium parameters

The program CHARMM is designed for molecular mechanics and dynamics calculations of macromolecules [20]. CHARMM has an extensive parameter set for the treatment of organic monomers, but does not contain many parameters for metallic species. It was therefore necessary to extend the existing force field to include the tricarbonylchromium(arene) moiety. First, we define the topology of the arene complex. The $Cr(CO)_3$ group was bonded to the benzyl via a dummy atom located at the centre of the benzene ring. We used a scheme similar to that of Doman et al. [29] when treating forces on the dummy atom. By placing the dummy atom at the centroid and 'bonding' it to the ring atoms, the forces on the dummy atom were equally distributed onto the ring carbons.

Appropriate equilibrium bond and angle values for the dummy atom were obtained from the crystal structure values listed in Table 2. The dummy atom was treated as an aromatic carbon atom, thus carbon-like force constants were applied to it. The mass of the dummy atom was assigned to be the same as that of carbon, but the van der Waals radius of the dummy atom was set to zero, to avoid the introduction of

Table 3
CHARMM atom classification

Name	Description
DUM	Dummy atom for centroid
CA	Aromatic carbon
CA1	Alternate aromatic carbon
MCR	Chromium metal atom
CM	Carbonyl carbon
OM	Carbonyl oxygen
DUM	Dummy atom for centroid

Table 4
Selected force-field bond parameters for Eq. (1)

Bond	k_b	r_0
MCR-CM	300.0	1.84
MCR–DUM	210.0	1.73
OM–CM	1115.0	1.14
CA1–DUM	305.0	1.41
CA–DUM	305.0	1.41

Table 5
Selected force-field angle parameters for Eq. (2)

	k_θ (kcal mol^{-1} rad^{-2})	θ_0 (°)		k_θ (kcal mol^{-1} rad^{-2})	θ_0 (°)
CM–MCR–CM	5.00	90.0	CA1–DUM–MCR	50.00	89.4
MCR–CM–OM	25.00	179.0	CA1–DUM–CA1	40.00	120.0
CM–MCR–DUM	5.00	126.2	CA1–DUM–CA	40.00	60.0
CA–DUM–MCR	50.00	90.0	CA–DUM–CA	40.00	120.0

non-existent interactions with the carbon atoms of the aromatic ring. Dihedral force constants for torsions involving the dummy atom were set to zero to allow free rotation of the chromium tricarbonyl group. The force constants for the metal dummy stretch and bend were assigned by analogy to similar metal dummy parameters already present in the force field [21].

Alternating carbons in the aromatic ring were by necessity assigned to different atom types (CA and CA1) for the purposes of construction; however, the force constants for the interactions involving CA were identical to those involving CA1, only the equilibrium angle values differing in a manner consistent with the crystal structure.

The carbonyl carbon and oxygen parameters were already present in the CHARMM force field [21]; these were used after checking to ensure that they did not deviate significantly from the crystal structure values. Force constants for bond stretch, angle bend and dihedral interactions involving the metal and the carbonyl group were obtained by analogy to other metal carbonyls present in the force field, or from the literature [29,30]. The non-bonded parameters were already present in the force field, with the exception of those of the dummy atom. A listing of CHARMM atom classifications is shown in Table 3. The newly added parameters are reported in Tables 4–7. A complete list of the CHARMM parameters has been published by MacKerell et al. [21] We found that torsion parameters involving the metal complex had small effect on the energy of the system as is often the case with this potential function. A free rotation about the dummy–chromium bond, unhindered by the potential form represented in Eq. (3), appeared to give qualitatively better results in the case of our conformational energy surface calculations.

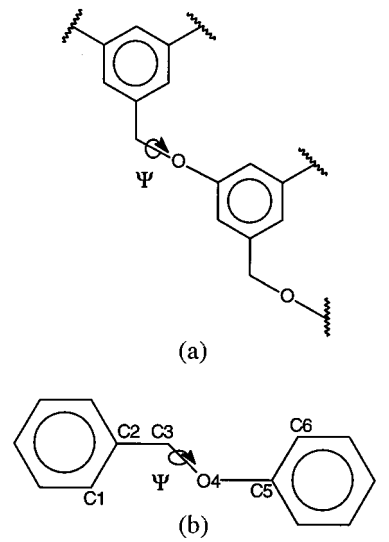

Fig. 3. (a) The ether linkage torsion angle Ψ as found in the poly(benzyl phenyl ether) dendrimer. (b) Benzyl phenyl ether model compound used in parameterisation of the ether linkage.

4.2. Parameterisation of ether linkage

In addition to the chromium parameters, a second area of force-field parameterisation was crucial to the accurate simulation of dendrimers. The ether linkage torsion angle Ψ, illustrated in Fig. 3(a), is present where surface groups are connected to the interior monomers, as well as in the links between internal monomers, and monomers to the central core molecule. It therefore has a significant effect on the topology of the macromolecule. Thus it is crucial that this torsion angle be parameterised properly in order for the simulation results to have any validity. The parameters for this torsion angle were adapted from the CHARMM polymer

Table 6
Dihedral parameters for metal-centred torsion angle rotations

Dihedral angle	k_ϕ(kcal mol^{-1} rad^{-2})	n	Phase [a]
CA–DUM–MCR–CM	0.155	6	180.0
CA1–DUM–MCR–CM	0.155	6	180.0
X–MCR–CM–X	0.05	4	0.000

[a] The phase is the minimum geometry of the dihedral.

Table 7
Selected non-bonded parameters for chromium complex **2**

	Polarizability	E	van der Waals radius
MCR	0.01	−0.020	1.465
CM	1.650000	−0.0262	2.
OM	0.84000	−0.1591	1.540
DUM	0.000000	−0.000000	0.000000

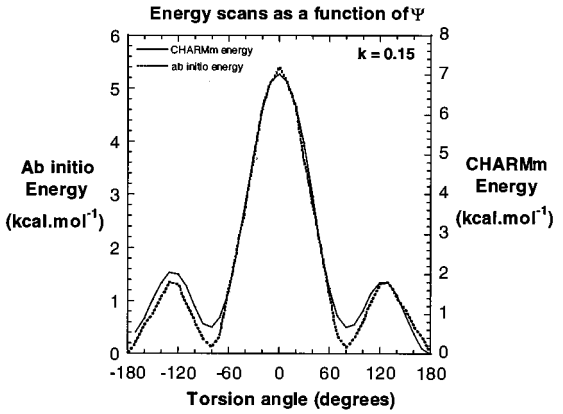

Fig. 4. The modified CHARMM and ab initio energy scans as a function of Ψ.

Table 8
Trial k_ϕ values with differences in barrier ratios and global maxima ratios from force field calculations and ab initio results

k_ϕ (kcal mol^{-1} rad^{-2})	Barrier ratio difference	Global maxima difference (kcal mol^{-1})
0.27	0.41	1.40
0.25	0.40	1.80
0.23	0.16	1.78
0.20	0.25	1.75
0.17	0.16	1.69
0.15	0.11	1.60

force field [22]. To ensure that this torsion is treated correctly, parameterisation was carried out by trial-and-error fitting of torsional rotation data to ab initio quantum mechanical data for a simple model compound, benzyl phenyl ether (Fig. 3(b)).

The molecular mechanical torsional potential as a function of Ψ (C2–C3–O4–C5) was obtained by varying Ψ through 360°, constraining at 10° intervals. At each Ψ value two aromatic ring conformations were varied. (C1–C2–C3–O4) and (C6–C5–O4–C3) were systematically varied from −180° to 180° at 30° intervals followed by steepest descents and conjugate gradients minimisation. Every permutation of the two ring orientations was explored for each value of Ψ, and the lowest-energy structure was recorded.

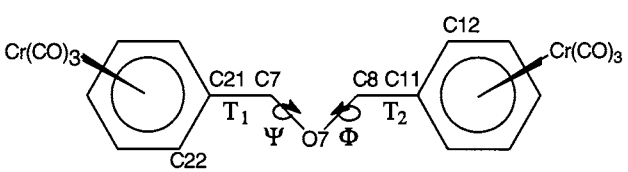

Fig. 5. The torsion angles Φ and Ψ for the energy map.

Table 9
Selected torsion angles from the two conformations

Torsion angle	XRAY	G_{MIN}
Φ (°)	−179.8	−180
Ψ (°)	175.6	180
T_1 (°)	−25.2	11.6
T_2 (°)	92.1	−85.9

Single-point ab initio energy calculations were carried out on each set of minimised coordinates resulting from the molecular mechanics calculations described above for the dihedral angle Ψ. We used GAUSSIAN94 [31] for all our ab initio calculations, which were performed at the Hartree–Fock level with the 6-31G(d) basis set. This produced the ab initio rotational potential for Ψ, which is shown with the molecular mechanics rotational potential for comparison in Fig. 4. The topology about the dihedral has three energy barriers as the carbon–carbon bond is rotated from −180° to 180°. The local maxima (−120° and 120°) occur where a hydrogen atom and a phenyl ring eclipse each other, while the global maximum (0°) occurs where two phenyl rings are eclipsed.

To parameterise the ether linkage torsion angle, the CHARMM data were fitted to the ab initio data, by changing the value of the coefficient k_ϕ in the torsional energy term of the force field, on a trial-and-error basis, starting with the initial value $k_\phi = 0.27$ kcal mol^{-1} rad^{-2}. The energy scans were compared using two criteria: the difference in the barrier height ratio, and the difference between the values of the global maxima. Trial k_ϕ values appear in Table 8, along with the two fitting criteria.

Overall, the best agreement with the ab initio data was found with $k_\phi = 0.15$ kcal mol^{-1} rad^{-2}. The barrier height ratio closely matches the ab initio ratio, and

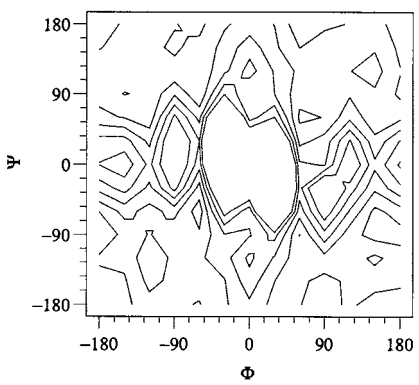

Fig. 6. The energy surface of chromium complex **2** as a function of Φ and Ψ, showing the global minimum near (−180, 180). Contours are at 2 kcal mol^{-1} intervals above the minimum.

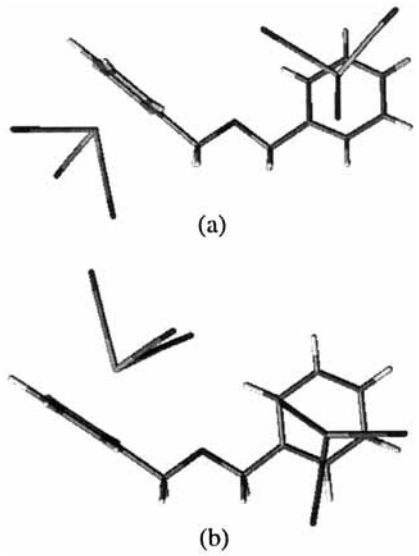

Fig. 7. (a) Conformation from crystal structure (XRAY) and (b) global minimum conformation from CHARMM conformational search (G_{MIN}).

the value of the global maxima are fairly similar. The original $k_\phi = 0.27$ kcal mol^{-1} rad^{-2} resulted in a better match of global maxima values, but a worse match for the barrier height ratio. The latter is the more important criterion, as it is a measure of the accuracy of the torsion angle contribution to the total potential, whereas the value of the global maxima is an indication of the accuracy of the entire parameter set.

5. Testing the force field

The accuracy of the new parameters was investigated by searching the conformational space of the $[Cr(CO)_3(C_6H_5CH_2OCH_2C_6H_5)Cr(CO)_3]$ complex for the lowest-energy conformer and then comparing this structure with the one found by single-crystal analysis described in Section 3.1 above. We perform a second test where we show that the experimental crystal structure can be accurately reproduced with the newly constructed force field.

Table 10
Selected dihedral angles from both crystal structure calculations

Dihedral	XRAY (vacuum)	XRAY (crystal)	G_{MIN} (vacuum)	G_{MIN} (crystal)
Φ (°)	−179.2	179.9	−180.0	−78.7
Ψ (°)	173.3	173.3	180.0	−152.4
T_1 (°)	−29.7	−29.7	11.6	−93.4
T_2 (°)	96.0	96.0	−85.9	−115.4

5.1. Mapping the energy surface of the dibenzyl ether bis-complex **2**

Using CHARMM, the global minimum conformation of the dibenzyl ether bis-complex **2** was found by mapping the energy surface of the molecule as a function of two torsion angles Φ (C11–C8–O7–C7) and Ψ (C21–C7–O7–C8) indicated on Fig. 5. Two additional torsion angles were taken into account when generating the energy surface, viz. T_1 (C22–C21–C7–O7) and T_2 (C12–C11–C8–O7). The latter torsion angles determine the orientation of the aromatic rings, for which several minimum-energy conformations could exist at each Φ/Ψ combination. Consequently at each interval, the lowest-energy local minimum was found by stepping through all of the T_1 and T_2 permutations at 30° intervals, followed by steepest descents and conjugate gradients minimisation algorithms.

Inspection of the resulting energy surface (Fig. 6) reveals the presence of high-energy barriers to rotation at $\Phi = 0°$ and $\Psi = 0°$, and the global minimum at $\Phi = -180°$, $\Psi = 180°$, indicating that the molecule adopts the fully extended conformation in the global minimum structure. The two phenyl rings (torsion angles T_1 and T_2) adopt *gauche* conformations. Table 9 lists the values of these dihedral angles for comparison with those found in the crystal structure. For simplicity from now on we refer to the global minimum conformer obtained from the energy surface as G_{MIN}, while the conformation of the crystallographic asymmetric unit is referred to as XRAY.

It is evident that although the G_{MIN} conformer approximates the XRAY conformer in terms of the primary dihedral angles Φ and Ψ, the two structures differ to quite a large extent in the ring torsion angle orientations (T_1 and T_2), with the result that the molecules adopt very different conformations (Fig. 7). The orientation of the right-hand-side aromatic rings in Fig. 7 is determined by the ring torsion angle T_1, whereas the aromatic ring on the left-hand side is controlled by T_2.

The changed sign for T_1 in G_{MIN} has little effect on the overall conformation. However, the value of T_2 (-85.9 as compared to $+92.1$ in XRAY) in the G_{MIN} structure results in the projection of the tricarbonylchromium group on the opposite face to that found in the XRAY structure. The XRAY conformer was minimised in vacuo, to relax the structure. Small adjustments were observed, but the molecule retained the same conformation, and therefore approximately the same values of Φ, Ψ, T_1 and T_2 (Table 10). G_{MIN} was found to be lower in energy than the minimised XRAY structure by 1.4 kcal mol^{-1}. This difference in energy can be ascribed to the molecule adopting a

higher-energy conformation in the crystal structure due to packing effects, as is demonstrated by the crystal structure calculations, which we discuss below.

5.2. Simulating the crystal structures

We simulated the crystal structure of the chromium complex **2** using the space group $P2_1/n$, the lattice parameters and the conformation (XRAY) from the crystal structure determination in two ways: first by fixing the experimentally determined lattice parameters and then secondly by optimising the lattice parameters within the CHARMM force field. Prior to the crystal structure simulation we minimised the two conformers in vacuo. This was followed by generating all symmetry-related images of the asymmetric unit within a cut-off of 999.0 Å.

The XRAY conformer is stabilised in the crystal by 11 kcal mol^{-1}, with no significant change in conformation (Table 10) when the lattice parameters are fixed. When we allowed the lattice parameters to optimise within the CHARMM force-field environment we observed a further 11 kcal mol^{-1} stabilisation energy. The main dihedral angles (T_1, T_2, Φ, and Ψ) were only changed by a few degrees and the cell parameters increased by 0.4 Å in the case of a and b while the dimension c showed a shift of approximately 0.9 Å from 23.562 to 24.458 Å. The small deviation of the CHARMM-simulated crystal structure from the experimentally determined lattice and molecular parameters is a good measure of the reliability of the force field. In future the non-bonded terms could possibly be further optimised when constructing a general organometallic force field to reduce the difference in CHARMM-simulated lattice parameters and those determined experimentally.

The G_{MIN} conformation was also simulated in the crystal structure environment, but does not pack well into the $P2_1/n$ space group due to close contacts between the asymmetric unit and the symmetry-related molecules. In order to eliminate close contacts but still pack into the same space group, a severe distortion of conformation is necessary (Table 10). The conformer obtained after minimisation in the lattice is thus very different from the G_{MIN} conformer, and has a molecular energy much higher (ca. 30 kcal mol^{-1}) than the corresponding XRAY crystal conformer, which is consistent with our expectation that G_{MIN} should be energetically disfavoured in this crystal environment. However, we note that the energy of the XRAY conformer in the crystal environment is more than 20 kcal mol^{-1} lower in energy than either the vacuum or G_{MIN} or XRAY conformers, which indicates that crystal packing is energetically favourable.

6. Conclusions

We have synthesised, characterised and determined the crystal structure of the novel complex $[Cr(CO)_3(C_6H_5CH_2OCH_2C_6H_5)Cr(CO)_3]$ (**2**). Using this crystal structure, we have constructed a force field suitable for molecular mechanics calculations of organochromium dendrimers. In addition the force field was further parameterised for the important benzyl ether linkage, by fitting molecular mechanics torsional rotation data to ab initio torsional data. By mapping the energy surface and simulating the crystal structure of the chromium complex **2**, we tested the parameter set. The structures produced from our molecular mechanics calculations compared well with those produced from single-crystal structure experiments and ab initio calculations. The force field we report here is suitable for molecular mechanics and dynamics calculations of organochromium small molecule complexes and poly(-benzyl phenyl ether) dendrimers.

7. Supplementary material

Crystallographic data for the structural analysis have been deposited with the Cambridge Crystallographic Data Centre, CCDC no. 133310 for compound **2**. Copies of this information may be obtained free of charge from: The Director, CCDC, 12 Union Road, Cambridge, CB2 1EZ, UK (Fax: +44-1223-336-033; email: deposit@ccdc.cam.ac.uk or www: http://www.ccdc.cam.ac.uk).

Acknowledgements

S.J.H., J.R.M. and K.J.N. wish to thank the University of Cape Town, the Foundation for Research Development (Pretoria) and AECI Ltd. for financial support. The authors wish to thank Professor J.A.K. Howard (University of Durham), for X-ray diffractometer time and contributions toward the crystal structure solution.

References

[1] R. Deschenaux, E. Serrano, A.-M. Levelut, Chem. Commun. (Cambridge) (1997) 1577.
[2] J.W.J. Knapen, A.W. van der Made, J.C. de Wilde, P.W.N.M. van Leeuwen, P. Wijkens, D.M. Grove, G. van Koten, Nature 372 (1994) 659.
[3] M.T. Reetz, G. Lohmer, R. Schwickardi, Angew Chem. Int. Ed. Engl. 36 (1997) 1526.
[4] C. Valério, J.-L. Fillaut, J. Ruiz, J. Guittard, J.-C. Blais, D. Astruc, J. Am. Chem. Soc. 119 (1997) 2588.
[5] S. Campagna, G. Denti, S. Serroni, A. Juris, M. Venturi, V. Ricevuto, V. Balzani, Chem. Eur. J. 1 (1995) 211.

[6] S. Achar, C.E. Immoos, M.G. Hill, V.J. Catalano, Inorg. Chem. 36 (1997) 2314.
[7] C. Cuadrado, M. Casado, B. Alonso, M. Morán, J. Losada, V. Belski, J. Am. Chem. Soc. 119 (1997) 7613.
[8] M. Hearshaw, J. Moss, Chem. Commun. (Cambridge) (1999) 1.
[9] Y.-H. Liao, J.R. Moss, J. Chem. Soc. Chem. Commun. (1993) 1774.
[10] F. Lobete, I. Cuadrado, C.M. Casado, B. Alonso, M. Moran, J. Losada, J. Organomet. Chem. 506 (1996) 109.
[11] R.L. Lescanec, M. Muthukumar, Macromolecules 23 (1990) 2280.
[12] W. Carl, J. Chem. Soc. Faraday Trans. 92 (1996) 4151.
[13] M.L. Mansfield, L.I. Klushin, J. Phys. Chem. 96 (1992) 3994.
[14] M.L. Mansfield, L.I. Klushin, Macromolecules 26 (1993) 4262.
[15] M. Murat, G.S. Grest, Macromolecules 29 (1996) 1278.
[16] A.M. Naylor, W.A. Goddard, Polym. Prepr. 29 (1988) 215.
[17] D.A. Tomalia, A.M. Naylor, W.A. Goddard, Angew. Chem. Int. Ed. Engl. 29 (1990) 138.
[18] J. Smith, C.B. Gorman, ACS PMSE Proc. 78 (1998) 226.
[19] K.J. Naidoo, S.J. Hughes, J.R. Moss, Macromolecules 32 (1999) 331.
[20] B.R. Brooks, R.E. Bruccoleri, B.D. Olafson, D.J. States, S. Swaminathan, M. Karplus, J. Comp. Chem. 4 (1983) 187.
[21] J. MacKerell, A.D. Bashford, M. Bellott, R.L. Dunbrack Jr., J.D. Evanseck, M.J. Field, S. Fischer, J. Gao, H. Guo, S. Ha, D. Joseph-McCarthy, L. Kuchnir, K. Kuczera, F.T.K. Lau, C. Mattos, S. Michnick, T. Ngo, D.T. Nguyen, B. Prodhom, I. Reiher, W.E.B. Roux, M. Schlenkrich, J.C. Smith, R. Stote, J. Straub, M. Watanabe, J. Wiorkiewicz-Kuczera, D. Yin, M. Karplus, J. Phys. Chem. B 102 (1998) 3586.
[22] K.J. Naidoo, K. Ueda, unpublished results (1998).
[23] F.H. Allen, O. Kennard, Chem. Des. Autom. News 8 (1993) 1–31.
[24] J. Blagg, S.G. Davies, N.J. Holman, C.A. Laughton, B.E. Mobbs, J. Chem. Soc. Perkin Trans. 1 (1986) 1581.
[25] G.M. Sheldrick, SADABS: Program for Scaling and Correction of Area Detector Data, University of Göttingen, Göttingen, Germany, 1996.
[26] G.M. Sheldrick, SHELXTL, Version 5/VMS, Madison, WI, Bruker Analytical X-ray Systems, 1995.
[27] W.D.S. Motherwell, PLUTO Plotting Program for Crystal Structures, Cambridge University, Cambridge, 1989.
[28] J.A. Labinger, in: M.J. Winter, E.W. Abel, F.G.A. Stone, G. Wilkinson (Eds.), Comprehensive Organometallic Chemistry, vol. 5, Pergamon Press, New York, 1995 (Chapter 8).
[29] T.N. Doman, C.R. Landis, B. Bosnich, J. Am. Chem. Soc. 114 (1992) 7264.
[30] J.W. Lauher, J. Am. Chem. Soc. 108 (1986) 1521.
[31] M.J. Frisch, G.W. Trucks, H.B. Schlegel, P.M.W. Gill, B.G. Johnson, M.A. Robb, J.R. Cheeseman, T.A. Keith, G.A. Petersson, J.A. Montgomery, K. Raghavachari, M.A. Al-Laham, V.G. Zakrzewski, J.V. Ortiz, J.B. Foresman, J. Cioslowski, B.B. Stefanov, A. Nanayakkara, M. Challacombe, C.Y. Peng, P.Y. Ayala, W. Chen, M.W. Wong, J.L. Andres, E.S. Replogle, R. Gomperts, R.L. Martin, D.J. Fox, J.S. Binkley, D.J. Defrees, J. Baker, J.P. Stewart, M. Head-Gordon, C. Gonzalez, J.A. Pople, Gaussian, Pittsburgh, PA, 1995.